Supplementary material

SARS-CoV-2 productively infects primary human immune system cells *in vitro* and in COVID-19 patients

Marjorie C Pontelli[1,†,*], Italo A Castro[1,†,*], Ronaldo B Martins[1], Leonardo La Serra[1], Flávio P Veras[2], Daniele C Nascimento[2], Camila M Silva[2], Ricardo S Cardoso[1], Roberta Rosales[4], Rogério Gomes[5], Thais M Lima[1], Juliano P Souza[1], Brenda C Vitti, Diego B Caetité[2], Mikhael H F de Lima[2], Spencer D Stumpf[7], Cassandra E Thompson[7], Louis-Marie Bloyet[7], Juliana T E Kawahisa[2], Marcela C Giannini[2,3], Letícia P Bonjorno[2,3], Maria I F Lopes[2,3], Sabrina S Batah[6], Li Siyuan[6], Rodrigo L Assad[2,3], Sergio C L Almeida[2,3], Fabiola R Oliveira[2,3], Maíra N Benatti[2,3], Lorena L F Pontes[5], Rodrigo C Santana[2,3], Fernando C Vilar[2,3], Maria A Martins[2,3], Pei-Yong Shi[7], Thiago M Cunha[2], Rodrigo T Calado[5], José C Alves-Filho[2], Dario S Zamboni[2,4], Alexandre Fabro[6], Paulo Louzada-Junior[2,3], Rene D R Oliveira[2,3], Sean PJ Whelan[8], Fernando Q Cunha[2], and Eurico Arruda[1,4,*]

[1] Virology Research Center, Ribeirao Preto Medical School, University of Sao Paulo, 14049-900, Ribeirao Preto, Sao Paulo, Brazil

[2] Center of Research in Inflammatory Diseases, Ribeirao Preto Medical School, University of Sao Paulo, 14049-900, Ribeirao Preto, Sao Paulo, Brazil

[3] Divisions of Clinical Immunology, Infectious Diseases and Intensive Care Unit, Ribeirao Preto Medical School, University of Sao Paulo, 14049-900, Ribeirao Preto, Sao Paulo, Brazil

[4] Department of Cell and Molecular Biology, Ribeirao Preto Medical School, University of Sao Paulo, 14049-900, Ribeirao Preto, Sao Paulo, Brazil

[5] Blood Center of Ribeirao Preto, 14049-900, Ribeirao Preto, São Paulo, Brazil

[6] Department of Pathology, Ribeirao Preto Medical School, University of Sao Paulo, 14049-900, Ribeirao Preto, Sao Paulo, Brazil

[7] Department of Biochemistry & Molecular Biology, the University of Texas Medical Branch, Galveston, TX 77555, USA

[8] Department of Molecular Microbiology, Washington University in St. Louis, Saint Louis, MO 63110, USA

[†] These authors contributed equally to this work.

[*] Correspondence to: Eurico Arruda, Virology Research Center, Ribeirao Preto Medical School, 3900 Bandeirantes Av, 14049-900, Ribeirao Preto, São Paulo, Brazil; Tel: +55 16-33153337; E-mail: eaneto@fmrp.usp.br; Marjorie Cornejo Pontelli, Washington University in St Louis, 660 S. Euclid Ave, 63110, St Louis, MO 63110, USA; Tel: +1 314/273-6812; E-mail: cmarjorie@wustl.edu; Ítalo de Araujo Castro, Washington University in St Louis, 660 S. Euclid Ave, 63110, St Louis, MO 63110, USA; Tel: +1 314/273-7027; E-mail: italo@wustl.edu

Supplementary Materials and methods

Production of mouse anti-SARS-CoV-2 hyperimmune serum

Male C57Bl/6 mice were bred and maintained under specific pathogen-free conditions at the Ribeirão Preto Medical School's animal facility, University of São Paulo. The production of mouse hyperimmune serum was carried out with 8-week-old male mice, following the institutional guidelines on animal experimentation ethics. It was approved by the University of São Paulo Ethics Committee for Animal Experimental Research (Protocol no. 001/2020-1). For animal immunization, virus stock was inactivated by adding formaldehyde to a final concentration of 0.02% with incubation overnight at 37°C. Viral particles were then purified by ultracentrifugation (10% sucrose cushion, 159.000× *g* for 1 h). The pellet was resuspended with hosphate Buffer Saline (PBS) 1x and stored at -20°C. To confirm inactivation, titration of the inactivated product was done both by $TCID_{50}$ and by plaque assay in Vero-E6 cells. After 5-day incubation, no discernible cytopathic effect was detected. Three C57Bl/6 mice were inoculated by the intramuscular route with an emulsion containing the equivalent of 10^6 $TCID_{50}$ of inactivated SARS-CoV-2 on complete Freund's adjuvant diluted 1:1 in PBS. Two boosts were given with inactivated SARS-CoV-2 in incomplete Freund's adjuvant on days 7 and 14 after the first immunization. One week after the last dose, animals were euthanized with an excess of anesthetics xylazine (60 mg/kg) and ketamine (300 mg/kg), followed by exsanguination by cardiac puncture. Animal seroconversion was evaluated by indirect immunofluorescence using slide preparations of SARS-CoV-2 infected Caco-2 cells, fixed with 4% paraformaldehyde and AlexaFluor 488-labeled rabbit anti-mouse secondary antibody. Coverslips were analyzed using an optic microscope (Olympus BX40).

RNA extraction and real-time RT-PCR

SARS-CoV-2 RNA detection by one-step real-time RT-PCR was done with primer-probe sets for SARS-CoV-2 according to the USA-CDC protocol, targeting the virus N1 gene and using the RNAse-P housekeeping gene as an internal control. Total RNA was extracted from 250 µl of homogenized cell pellets and supernatants from in vitro assays with Trizol. All real-time PCR assays were done on a Step-One Plus thermocycler (Applied Biosystems). Viral loads of SARS-CoV-2 were determined using a standard curve prepared with a plasmid containing all three targets for the sets of primers/probes designed by CDC protocol (N1, N2, and N3), inserted into a TA cloning vector.

Fluorescent in situ hybridization (FISH)

Fluorescent in situ hybridization (FISH) was performed using an oligonucleotide probe targeting the N2 gene from the SARS-CoV-2 replicative intermediate negative-strand RNA. The FISH protocol

was adapted from published procedures (Planell-Saguer et al., 2010). Slides were examined in a Zeiss LSM 780 confocal microscope (Zeiss, Germany) using × 63 NA 1.4 oil-immersion objective.

Supplementary references

Planell-Saguer, M. De, Rodicio, M.C., and Mourelatos, Z. (2010). Rapid in situ codetection of noncoding RNAs and proteins in cells and formalin-fixed paraffin-embedded tissue sections without protease treatment. Nat. Protoc. *5*, 1061–1073.

Xie, X., Muruato, A., Lokugamage, K.G., et al. (2020). An infectious cDNA clone of SARS-CoV-2. Cell Host Microbe *27*, 841–848.e3.

Supplementary Tables

Supplementary Table S1 COVID-19 patient characteristics.

Demographics		**%**
Number	29	
Age (years)	61.89 ±17.10	
Hospital stay (days)	9.35 ±4.138	
Female	13	44%
Comorbidities		
Hypertension	16	55%
Diabetes	13	44%
Obesity	13	44%
Lung disease	4	14%
History of smoking	9	31%
Heart disease	7	24%
Kidney disease	2	7%
History of stroke	2	7%
Cancer	4	14%
Autoimmune diseases	2	7%
Immune deficiency	2	7%
Laboratorial findings		
CRP (mg/dl)*	14.41 ±8.11	
D-Dimers (μg/ml)**	2244 ±1698	
LDH (U/L)[#]	749,4 ±490,5	
Ferritin (ng/ml)[&]	1985 ±2836	
Haemoglobin (g/dl)	12.16 ±2.62	
Neutrophils (cell/mm^3)	7521 ±4952	
Lymphocytes (cell/mm^3)	1666 ±1286	
Platelets (count/mm^3)	231009 ±136433	
Image findings (n)	29	100%
Medications		
Antibiotics	29	100%
Heparin	29	100%
Hidroxicloroquine	3	10%
Oseltamivir	11	37%
Glucocorticoids	16	55%
Respiratory status		
Mechanical ventilation	24	83%
Nasal-cannula oxygen	27	93%
Room air	0	
pO_2	70.36 ±45.64	
O_2 saturation	82.71 ±18.58	
Outcome		
Deaths	9	31%

*CRP: C-reactive protein (normal value <0.5 mg/dl); **D-dimers (normal value <0.5 μg/ml); [#]LDH: lactic dehydrogenase (normal range 120–246 U/L); [&]Ferritin (normal range 10–291 ng/ml).

Supplementary Table S2 Viral loads of SARS-CoV-2 in PBMCs from COVID-19 patients tested by real-time RT–PCR.

Patient ID	Genome copies/total RNA (μg)
P39	68560
P42	22770
P43	20782
P45	36507
P46	22140
P47	94736
P48	26455
P50	16396
Mean ±SD	**38543 ±28114**

Supplementary Table S3 Key resources.

Reagent or resource	Source	Identifier
Antibodies		
Fixable Viability Dye eFluor™ 780	(eBioscience)	
Anti-human CD4	Abcam	Cat. 133616 clone EPR6855
Anti-human CD8	Abcam	Cat. ab4055
Anti-human CD14	Abcam	Cat. ab133335 clone EPR3653
Anti-human CD19	Abcam	Cat. ab134114 clone EPR5906
Anti-human CD20	Abcam	Cat. ab27093
Anti-dsRNA J2	Scicons	Cat. 10010500
Anti-human IgG	Sigma-Aldrich	Cat. B-1140
Donkey anti-mouse IgG-Alexa Fluor® 488	Thermo Fisher	Cat. a-21202
Goat anti-mouse (IgG) Alexa Fluor® 647	Abcam	Cat. 150115
Goat anti-rabbit (IgG) Alexa Fluor® 647	Abcam	Cat.150079
Anti-GM130	BD	Cat. 610822
Anti-human CD3-APC	eBioscience	Cat. 17-0036-42
Anti-human CD4 PerCP-Cy5.5	BD	Cat. 560650
Anti-human CD8 PE-Cy7	BD	Cat. 557746
Anti-human CD19 APC	BioLegend	Cat. 302212
Anti-human CD14 PerCP	Abcam	Cat. ab91146
Anti-human CD16 PE	eBioscience	Cat. 12-0168-42
Anti-human CCR2 Brilliant Violet 421	BioLegend	Cat. 357210
Anti-human IL-6	BD	Cat. 554400 clone MP5-20F3
Anti-mouse IgG-Alexa Fluor® 488	Thermo Fisher	Cat. a-21202
Anti-rabbit IgG	Abcam	Cat. 64256
Anti-rat IgG	Vector	Cat. BA4000

Anti-respiratory syncytial virus antibody	Abcam	Cat. ab20745
Anti-Digoxigenin/Digoxin	Vector	Cat. MB-7000
Anti-human ACE2 antibody	Rhea Biotech R&D Systems	Cat. IM-0060 Cat. AF933
Horse anti-mouse secondary antibody	Vector (part of Vectastain® ABC Kit)	Cat. BA-2000

Viruses

SARS-CoV-2 Brazil/SPBR-02/2020	Laboratory of Edison Luiz Durigon (ICB-USP, São Paulo)	
Infectious clone SARS-CoV-2 with reporter neonGreen (icSARS-CoV-2)	Laboratory of Michael Diamond (Washington University in St Louis)	Described in Xie et al. (2020)

Chemicals

Camostat	Sigma-Aldrich	Cat. SML0057
Percoll	GE Healthcare	
NH_4Cl	Sigma Aldrich	
Trizol®	Invitrogen	
Poly-Lysine	Sigma-Aldrich	

Commercial Kits

Streptavidin-peroxidase polymer	Sigma-Aldrich	Cat. S2438
Vector AEC peroxidase system	Vector	Cat. SK-4200
FLICA 660 Caspase-3/7 Assay Kit	ImmunoChemistry Technologies	Cat. 9125
ApoScreen AnnexinV-FITC apoptosis kit	SouthernBiotech	
TaqPath 1-Step qRT-PCR Master Mix	Applied Biosystems	
TSA Cyanine 3 System	Perkin Elmer	Cat. NEL704A001KT

Recombinant DNA (sequences and plasmids)

Plasmid, PTZ57R/T CloneJetTM Cloning Kit	Thermo Fisher
Synthetic, SARS-CoV Urbani strain (GenBank AY278741.1)	Integrated DNA Technologies
Synthetic, codon optimized SARS-CoV-2 Wuhan-Hu-1 (GenBank MN908947.3)	Integrated DNA Technologies
Synthetic, MERS-CoV HCoV-EMC/2012 spike sequence (GenBank NC_019843.3)	Integrated DNA Technologies

Oligonucleotides sequences

N2 gene sequence 5’-TTACAAACATTGGCCGCAAA-3’	Integrated DNA Technologies

Supplementary Figures

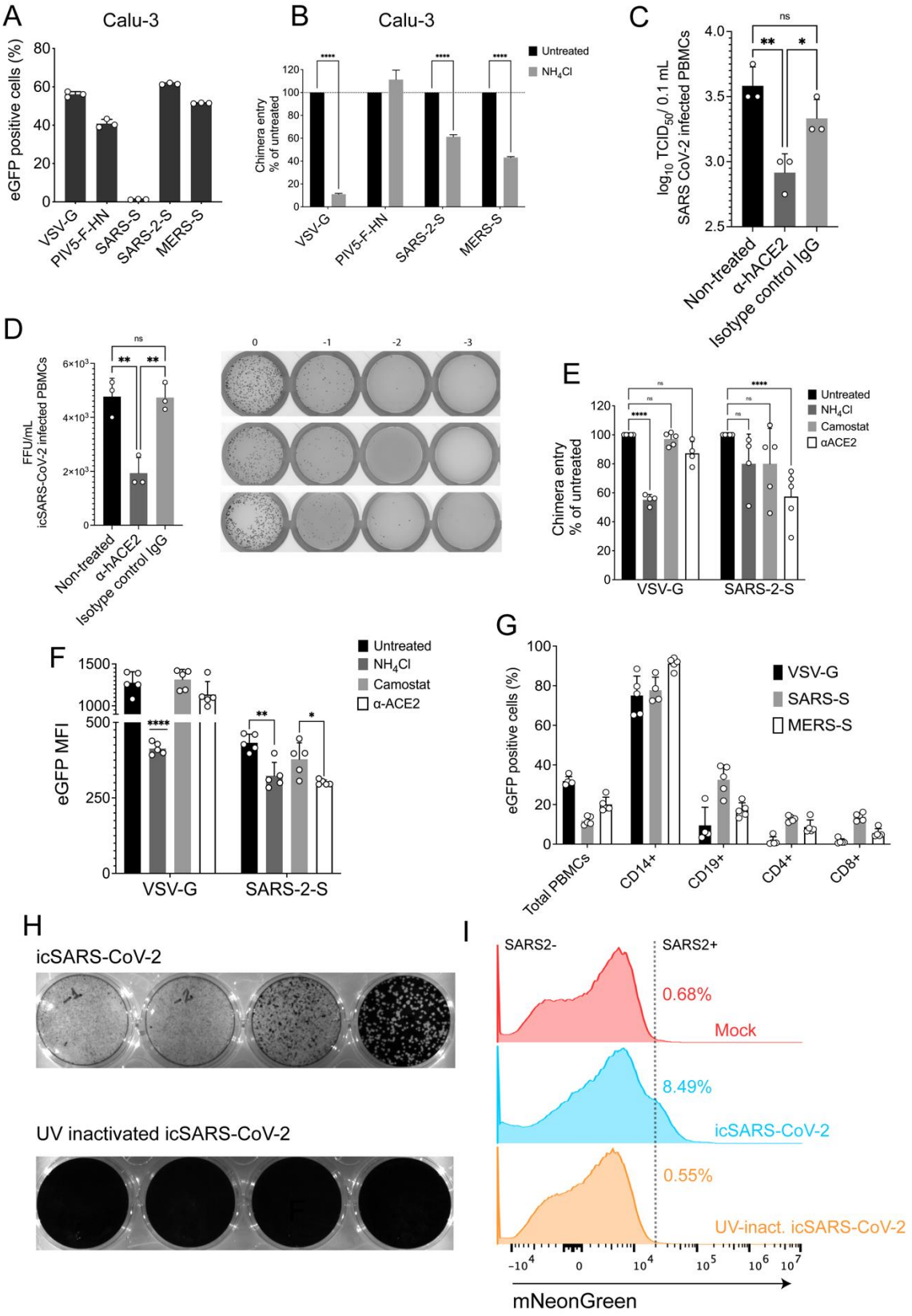

Supplementary Figure S1 VSV chimera viruses and icSARS-CoV-2 infection controls. (**A**) Frequencies of Calu-3 cells eGFP-positive. PBMCs were infected with VSV with the native G glycoprotein, or chimeras bearing the F (fusion) and HN (hemagglutinin) protein from parainfluenza 5 virus (PIV), or spike protein from

SARS-, SARS-2- or MERS-CoV. 8hpi cells were fixed and analyzed by flow cytometry. (**B**) Ammonium chloride treatment in Calu-3. PBMCs were treated with 20 μM NH_4Cl 20 min before infection. Cells were then infected with the different chimera viruses in presence of NH_4Cl. After 8hpi cells were fixed and analyzed by flow cytometry. (**C** and **D**) SARS-CoV-2 progeny production quantification of infected PBMCs pre-treated with anti-hACE2 or unrelated IgG isotype control. PBMCs were pre-treated with anti-hACE2 or IgG isotype control and infected with either SARS-CoV-2 (**C**) or icSARS-CoV-2 (**D**). After 24 hpi, the resulting progeny was read out by $TCID_{50}$ (**C**) or FFU (**D**). (**E** and **F**) Frequency (**E**) and mean fluorescence intensity (**F**) of VSV-G or SARS-2-S-infected PBMCs after entry inhibition treatments. PBMCs from healthy donors were pre-treated with NH_4Cl, camostat mesylate, or anti-hACE2 and then infected with VSV-G or VSV-SARS-2-S. After 8 hpi, cells were fixed and analyzed by flow cytometry. (**G**) Subpopulations' frequencies of eGFP positive cells after infection with VSV chimera reporter viruses. VSV-G and chimeras SARS-, or MERS-CoV-S were used to infect PBMCs from healthy donors. 8hpi cells were fixed, stained for different cell phenotypes, and analyzed by flow cytometry. The percentage of each cell subtype was normalized to the total PBMC value. (**H**) icSARS-CoV-2 stock titration and UV-C inactivation confirmation by plaque assay. (**I**) Histogram of mNeonGreen intensity after PBMC infection with mock-, icSARS-CoV-2 and UV-inactivated icSARS-CoV-2. Significance was analyzed by one-way ANOVA with Bonferroni's post-test. *$P < 0.05$, ***$P < 0.001$, ****$P < 0.0001$.

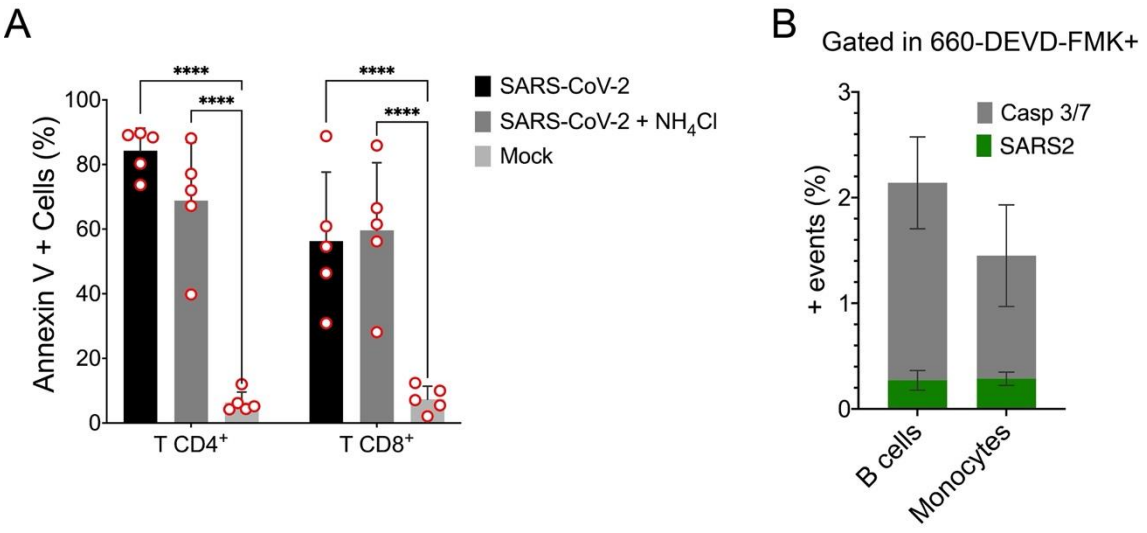

Supplementary Figure S2 Apoptosis markers' staining in PBMCs. (**A**) Percentage of lymphocytes expressing phosphatidylserine (PS) on the surface after *in vitro* infection with SARS-CoV-2. PBMCs were infected with SARS-CoV-2, with or without 20 mM NH_4Cl pretreatment and 24hpi, cells were stained with annexin-V. Analysis was made independently of Live/Dead APC/H7 staining. (**B**) Percentage of monocytes and B cells with active caspases 3/7 (gray) after infection with icSARS-CoV-2 (green). PBMCs were infected with icSARS-CoV-2 and 24hpi, cells were stained with 660-DEVD-FMK FLICA for 1h, fixed and analyzed by flow cytometry. Mean ± SD is shown for all bar graphs. Significance was determined by one-way ANOVA and Bonferroni's post-test was applied.

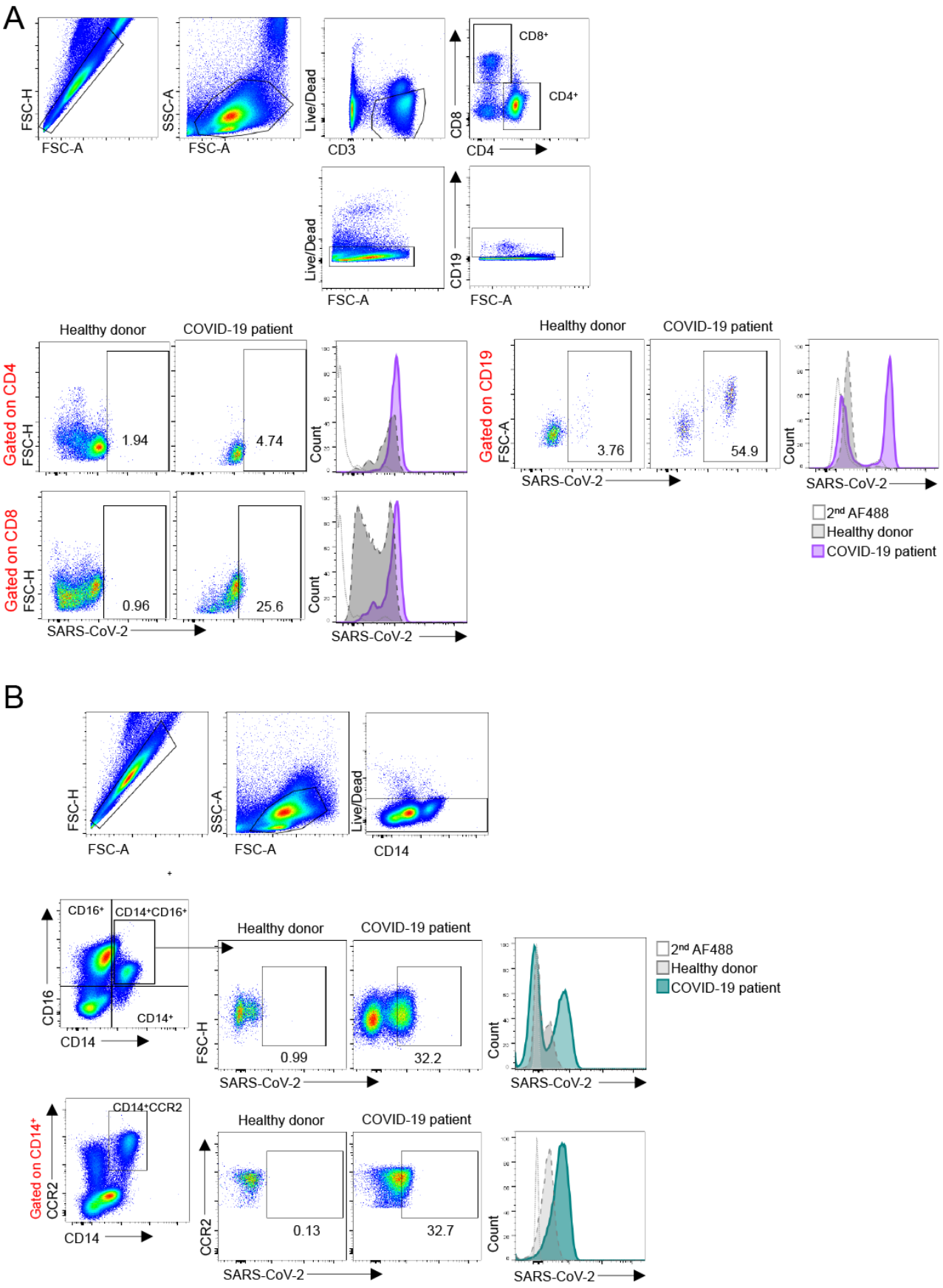

Supplementary Figure S3 Flow cytometry analysis and gating strategies used for immunophenotyping SARS-CoV-2 naturally infected cells. (**A**) Cells were initially gated to exclude doublets and to exclude dead cells, using Live/Dead APC/H7 and CD3 staining. Next, detection of SARS-CoV-2 antigens in live T

lymphocytes was defined based on the background secondary antibody signal (Alexa488) and signal obtained in healthy donors (flow plots and representative histograms). The same strategy was used for $CD19^+$ B lymphocytes. (**B**) Live monocytes were initially gated as described for lymphocytes. Next, expression of CD14 and CD16 was used to define circulating monocyte subpopulations. Expression of CCR2 by $CD14^+$ and $CD14^+CD16^+$ cells was used to define inflammatory monocytes. Among every defined subpopulation, expression of SARS-CoV-2 antigens was defined in comparison with secondary antibody background and healthy donors staining (flow plots and representative histograms).

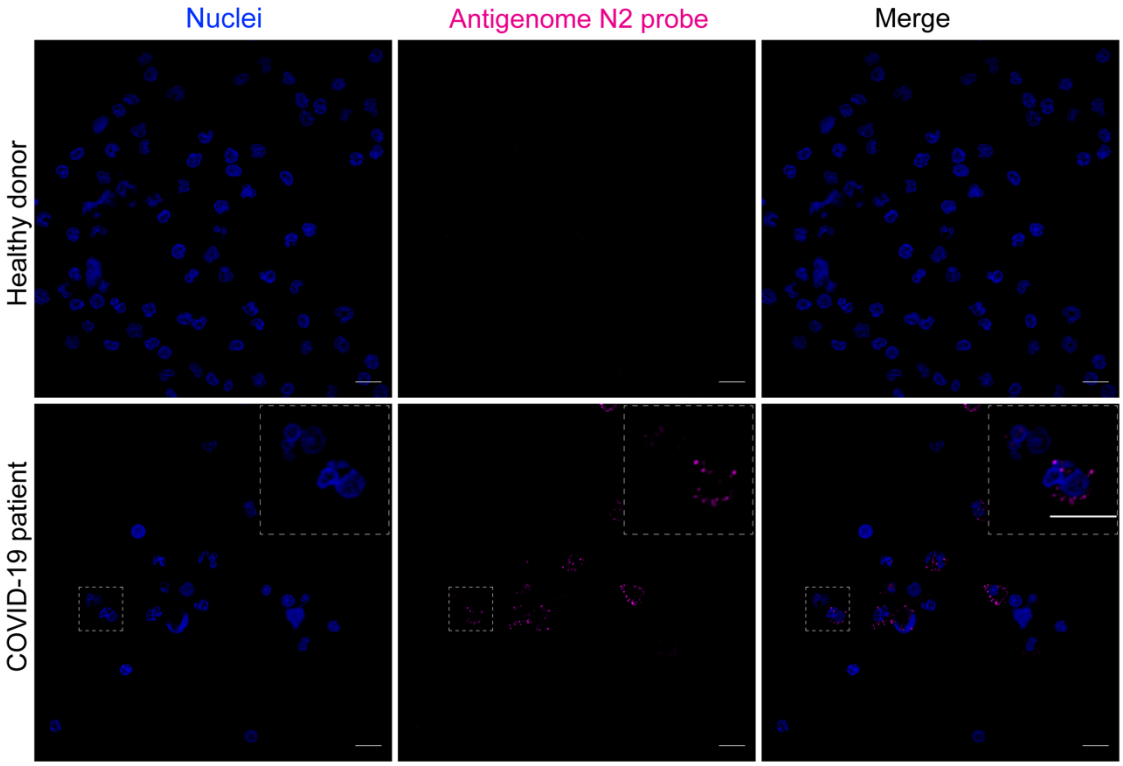

Supplementary Figure S4 SARS-CoV-2 antigenome detection in PBMCs from COVID-19 patients. PBMCs from COVID-19 patient and a matched-healthy donor control were fixed and processed for detection of SARS-CoV-2 antigenome N2 probe (magenta) and nuclei (blue). Coverslips were analyzed using confocal microscopy. Magnification 630×. Inset zoom 4×. Scale bar, 5 μm.

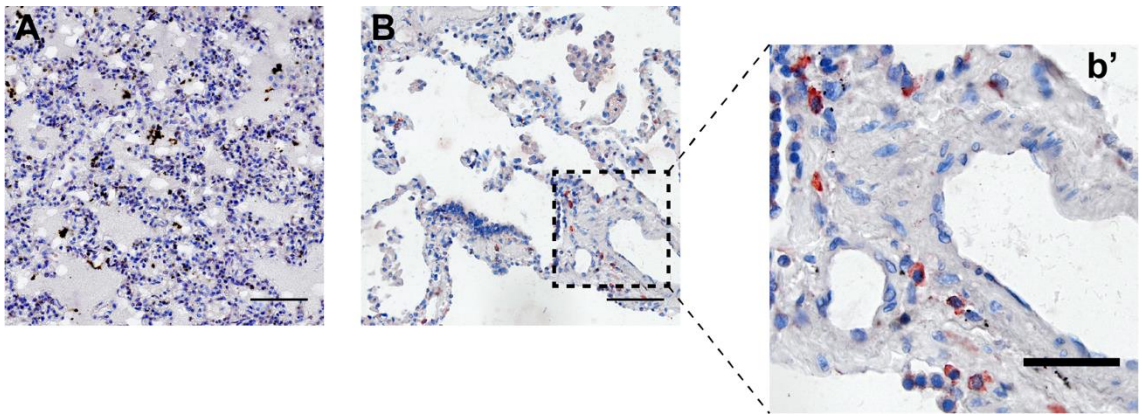

Supplementary Figure S5 Immunohistochemistry for SARS-CoV-2 antigens in post mortem lungs from COVID-19. (**A**) Post mortem lung fragment from a hantavirus fatal case obtained in 2016, as a negative control for SARS-CoV-2 staining. (**B**) Staining for SARS-CoV-2 in lung from COVID-19 fatal case. (**b'**) Individual cells showing strong cytoplasmic staining for SARS-CoV-2 antigens in detail. Magnification 400×. Scale bar, 50 µM.

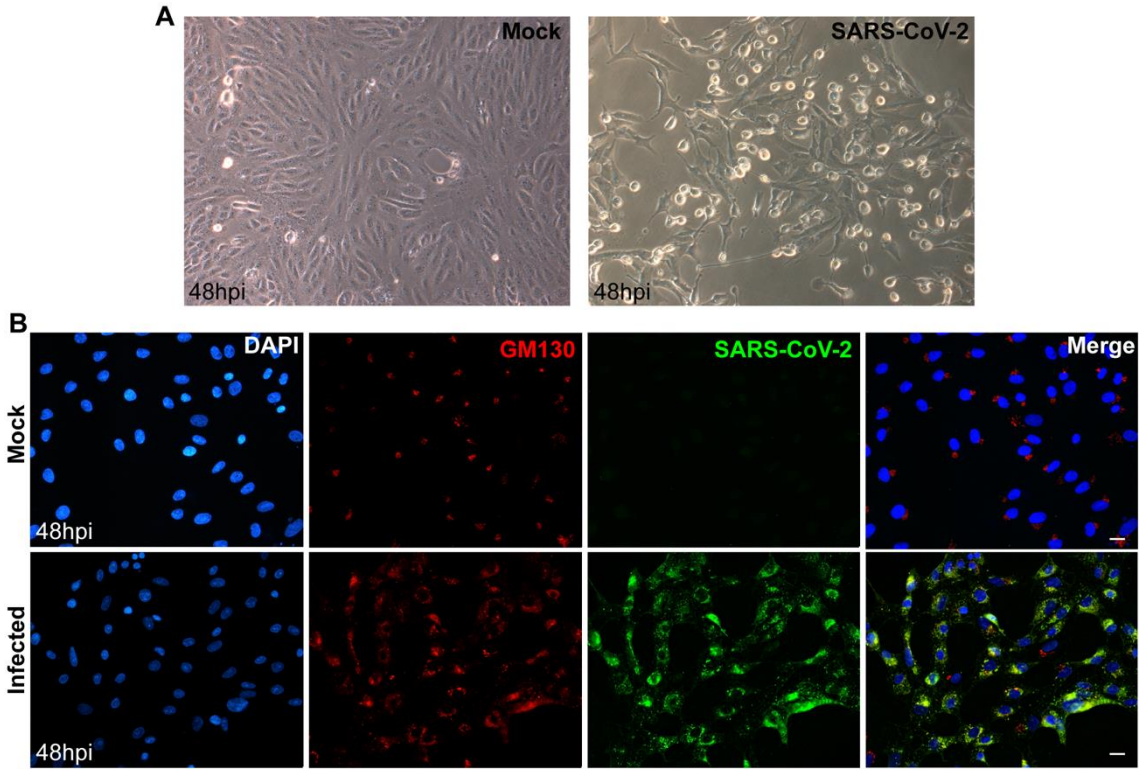

Supplementary Figure S6 Validation of SARS-CoV-2 detection with human convalescent serum. Vero cells were infected with SARS-CoV-2 (MOI=1) or mock and incubated for 48 h. (**A**) Phase-contrast microscopy of uninfected (left panel) and SARS-CoV-2-infected (right panel) Vero cell monolayers with cytopathic effect (magnification 400×). (**B**) Immunofluorescence of Vero cells infected with SARS-CoV-2 or mock-treated at 48 hpi, when cells were fixed and stained for GM130 (red), virus (green) and nuclei (DAPI). Scale bar, 10 µm.

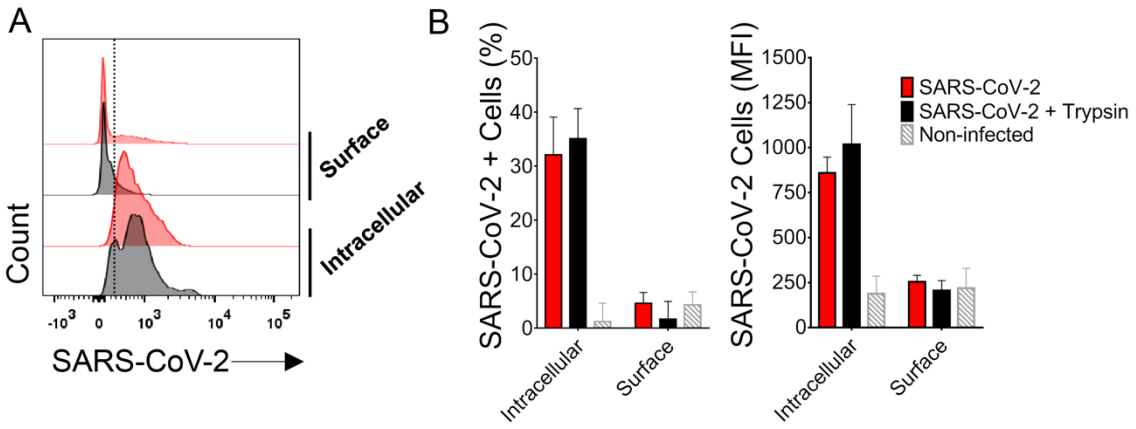

Supplementary Figure S7 Flow cytometry (FC) of SARS-CoV-2-infected PBMCs from healthy donors with labeling for SARS-CoV-2. PMBCs from healthy donors infected in vitro (MOI=1) were analyzed by FC using mouse polyclonal anti-SARS-CoV-2 with and without cell permeabilization. Treatment with trypsin to remove surface-bound viral particles was used as an additional control. (**A**) Representative histograms of surface and intracellular staining for SARS-CoV-2, with SARS-CoV-2-infected cells in red and trypsin-treated infected cells in black. (**B**) Comparison of intracellular and surface staining of infected cells treated or not with trypsin, and non-infected cells in percentages on the left and MFI on the right.

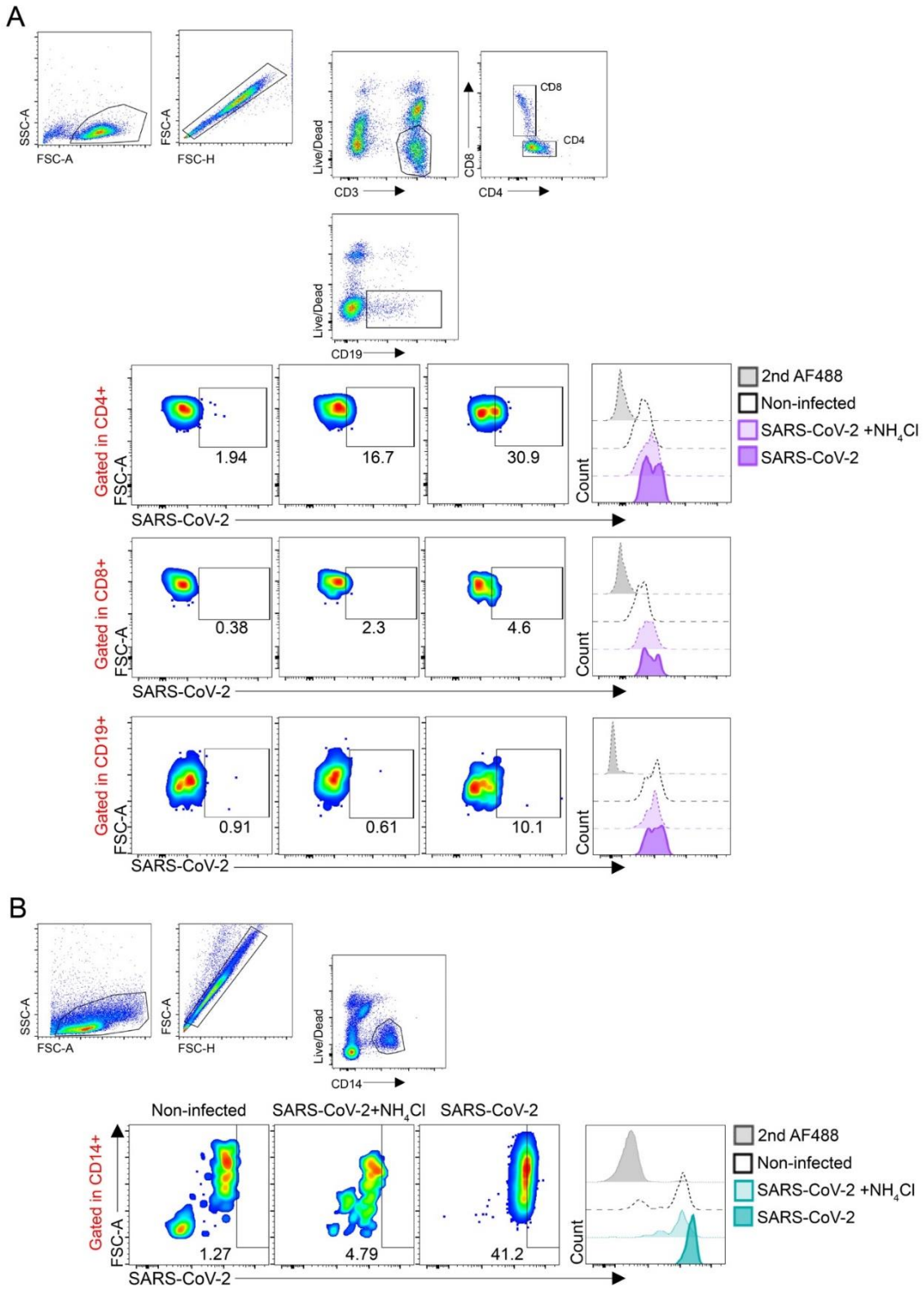

Supplementary Figure S8 SARS-CoV-2 differentially infects subsets of human PBMCs *in vitro*. Representative flow cytometry plots of PBMCs infected with SARS-CoV-2 (24 hpi) in the presence or absence of 20 mM NH_4Cl with gating in live lymphocytes (**A**) ($CD4^+$, $CD8^+$ or $CD19^+$ cells) or live monocytes (**B**) ($CD14^+$ cells). Representative histograms of the fluorescence for each condition in comparison with the proper controls. The gray-shaded curve indicates secondary antibody Alexa488 signal background, while the dashed curve indicates the background signal in mock-infected cells. The light- and dark-colored curves indicate respectively cells infected in the presence and absence of NH_4Cl.